A novel parametric impeller design framework for helium turbo-expanders: validation via omega vortex characterization in hydrogen liquefaction

Hongmin Liu[1,2], Yanan Li[1,2], Jiansheng Zuo[1,2], Changlei Ke[1,*], Kongrong Li[1,], Xiaohua Zhang[1], Lianyou Xiong[1], Nan Peng[1] and Liqiang Liu[1,2]**

[1] Key Laboratory of Cryogenic Science and Technology, Technical Institute of Physics and Chemistry, Chinese Academy of Sciences, Beijing, 100190, China
[2] University of Chinese Academy of Sciences, Beijing, 100049, China

[*]E-mail: kechanglei@mail.ipc.ac.cn
[**]E-mail: krli@mail.ipc.ac.cn

Abstract. This study proposes a novel Cylindrical Projection-Based Parametric Impeller Design (CPPID) framework for helium turbo-expanders in cryogenic hydrogen liquefaction. The CPPID method decouples the radial-to-axial curvature transitions at hub, center, and shroud layers, enabling precise and independent control of the three-dimensional blade geometry. The optimization process, guided by the Omega (Ω) vortex identification criterion, aimed at minimizing flow losses within the impeller passage. The application of this method led to a measurable performance improvement for the turbo-expander. The isentropic efficiency was raised from 92.96% to 93.39% under demanding conditions, building upon an already high performance baseline. This efficiency gain, albeit incremental, is substantiated by a marked suppression of large scale vortices ($\Omega = 0.8$) at the mid-span region, confirming enhanced flow stability.

1. Introduction

Hydrogen, as an efficient and clean secondary energy carrier, is crucial for achieving carbon neutrality[1]. Its large-scale storage and transport rely on low temperature liquefaction, which increases its volumetric energy density nearly 800 times[2]. The helium turbo-expander (HTE) is the core refrigeration component in this process, whose isentropic efficiency directly determines the plant's energy consumption. As flow losses within the impeller passage account for the largest portion of total losses in an HTE, optimizing the impeller design is paramount for enhancing efficiency.

Conventional design methods, often based on mean-line analysis or black-box commercial software optimization, lack precise control over the three dimensional blade geometry and its direct link to internal flow physics[3, 4]. To address this limitation, this study proposes a novel Cylindrical Projection-Based Parametric Impeller Design (CPPID) method. CPPID enables precise control of blade profile geometry at key spanwise sections and ensures smooth transitions, aiming to generate a 3D impeller geometry that better aligns with ideal flow structures.

To validate the CPPID method, the final-stage HTE from a 5 tons per day hydrogen liquefaction plant[5], which has an experimentally validated overall efficiency of 84.4%, was selected as a high performance baseline. The original impeller from this plant was replaced and

redesigned using the CPPID framework, preserving key dimensions to ensure compatibility. The performance of the CPPID-designed impellers is evaluated against a baseline impeller generated by the CPPID method itself, thereby isolating and highlighting the effect of parametric optimization.

2. Simulation model

Simulations are carried out on a single flow passage of the cryogenic helium turbo-expander, including both the nozzle and impeller. The fluid domains for the nozzle and impeller are modeled in ANSYS-CFX.

To fairly evaluate the impact of parametrically designed blade shapes on the turbo-expander's performance, all comparative simulations in this study were conducted under a consistent meshing strategy. **Figure 1** demonstrates the grid independence verification for the baseline configuration, The total node count is 2.1 million, with 0.85 million for the nozzle and 1.25 million for the impeller. While the absolute node count varied slightly across different impeller geometries, all designs maintained a highly consistent mesh quality, ensuring that performance differences can be directly attributed to geometric variations rather than numerical discrepancies. The dimensionless y^+ is set to 1.1 to control the thickness of grid cells near the wall, ensuring it is small enough to resolve the boundary layer[6]. The SST model is compatible with turbulence models that rely on y^+, as it automatically selects the appropriate near-wall function based on different y^+ values. This established mesh topology and resolution, including the y^+ criterion, were subsequently applied to all impeller variants investigated in this parametric study. The nozzle was set as a stationary domain, while the impeller was set as a rotating domain. Both the nozzle and impeller flow passages had adiabatic, no-slip walls. A frozen rotor interface was chosen between the rotating and stationary domain. This study also employs a real gas model for the computational fluid dynamics (CFD) simulations of cryogenic helium flow. Specifically, a Real Gas Property (RGP) file was utilized within the ANSYS CFX solver to accurately represent helium's thermodynamic properties. The RGP file functions as a high fidelity data table containing key properties such as enthalpy, entropy, specific volume, speed of sound and so on. ANSYS CFX accesses this pre-computed table during simulations, which is a more accurate method.

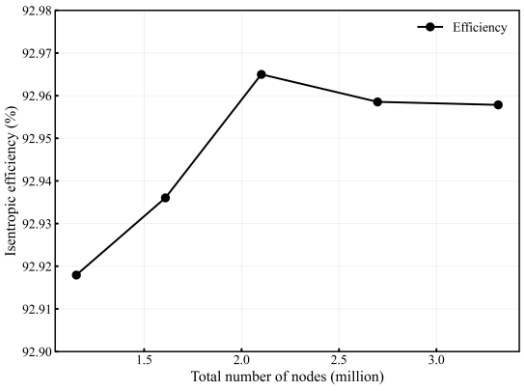

Figure 1. Grid independence verification of the baseline configuration.

3. METHODOLOGY

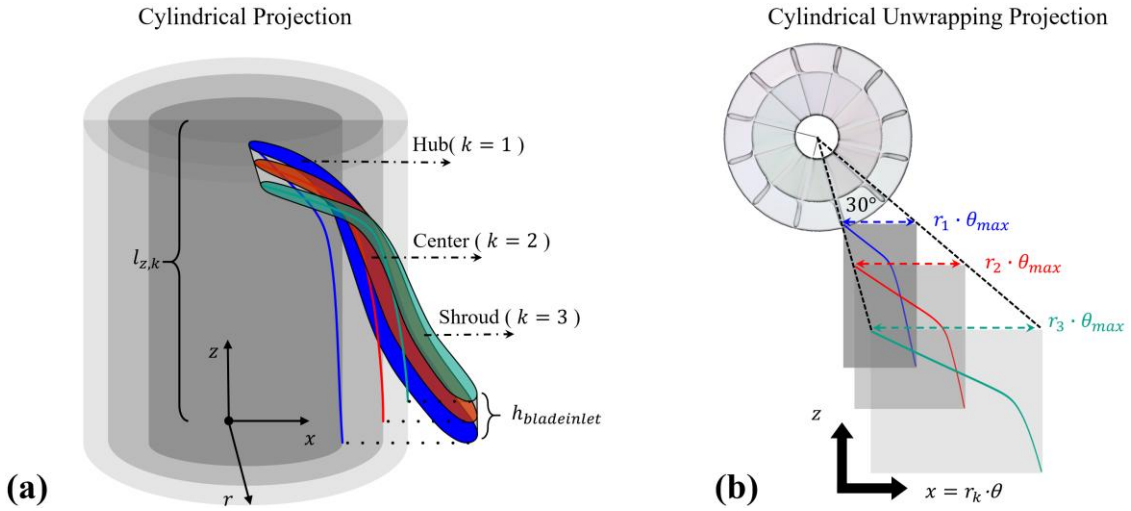

Figure 2. Cylindrical Projection-Based Parametric Design of Impeller Layers. Projection of blade curves onto cylindrical surfaces and unwrapping

3.1 Cylindrical Projection-Based Parametric Impeller Design(CPPID)

This paper introduces a Cylindrical Projection-based Parametric Impeller Design (CPPID) method for the direct control of 3D flow passage geometry. As shown in **Figure 2(a)**, the blade is abstracted into three key spatial curves at the hub, center (mid-span), and shroud. The core of CPPID involves projecting each curve onto a cylindrical surface defined by its respective outlet radius r_k (where $k = 1, 2, 3$). This cylindrical surface is then unwrapped into a plane with coordinates z (axial) and x (circumferential, $x = r_k \cdot \theta$).

On this unwrapped plane, the profile of each curve is governed by the parametric equation:

$$z = l_{z,\ k} - T_u \cdot x - l_{z,\ k} \cdot (tanh(T_r \cdot (x - x_{max,\ k}))) \quad (1)$$

Here, $l_{z,k}$ is the projected axial length for layer k, calculated as:

- Hub $(k = 1) : l_{z,1} = L_z$
- Center $(k = 2) : l_{z,2} = L_z - 0.5 \cdot h_{bladeinlet}$
- Shroud $(k = 3) : l_{z,3} = L_z - h_{bladeinlet}$

Where $L_z = 19.5$ mm is the impeller's axial length, $h_{bladeinlet} = 5.77$ mm is the blade height at the inlet. The term $x_{max,k} = r_k \cdot \theta_{\max}$ defines the maximum unwrapped length, with $\theta_{\max}$ fixed at 30° in this study, see **Figure 2(b)**.

Two key design parameters, T_u (Turning) and T_r (Transition), govern the curve shape. In this study, the design parameter T_u, which governs the outlet flow slope and turning capability, was held constant. This allows for a focused investigation into the influence of the transition parameter T_r. As illustrated in **Figure 3**, T_r controls the sharpness of the flow transition from the radially dominated to the axially dominated region within the blade passage. A higher T_r value produces a sharper transition with a more rapid curvature change, whereas a lower T_r value yields a smoother, more gradual transition.

To demonstrate the effectiveness of the CPPID method, an initial impeller geometry was generated using a uniform set of parameters, with the transition parameters T_r for all three layers (hub, center, shroud) set to 2 and the turning parameters T_u set to 3. This initial design retained the fundamental dimensions (axial length, blade height, outlet radius) of the baseline impeller

from the 5 tons per day hydrogen liquefaction plant, ensuring consistency in operational conditions and nozzle configuration. The optimization process involved systematically adjusting the transition parameter T_r at each layer while holding the turning parameter T_u constant.

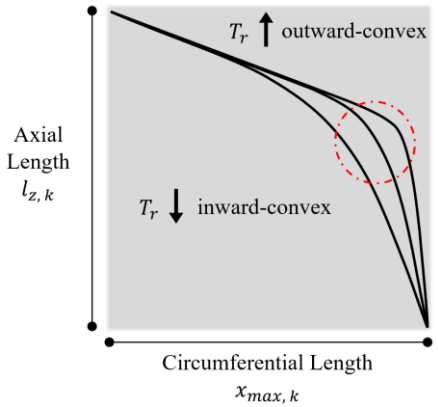

Figure 3. Effect of parameters T_r on the blade profile curve shape in the cylindrical projection

3.2 Vortex identification method

The intricate flow dynamics within turbo-expanders demand precise identification of vortical structures to localize energy loss mechanisms and guide aerodynamic optimization. Vortex identification methodologies have evolved through three generations, each addressing limitations of its predecessors. First-generation methods rely solely on vorticity magnitude ($\nabla \times V$), which inadequately distinguishes true vortices from shear dominated regions such as boundary layers. Second-generation approaches, including Q criterion, λ_2 criterion, Δ criterion, λ_{ci} criterion, utilize eigenvalue analysis but require arbitrary thresholds to isolate vortices, thereby overlooking fine-scale turbulent structures. To overcome these shortcomings, this study adopts the third-generation Ω method[7], which quantifies the dominance of rotational motion over strain deformation. The Ω parameter is defined as:

$$\Omega = \frac{\|B\|_F^2}{\|A\|_F^2 + \|B\|_F^2 + \varepsilon} \tag{2}$$

$$A = \frac{1}{2}(\nabla V + \nabla V^T) = \begin{bmatrix} \frac{\partial u}{\partial x} & \frac{1}{2}\left(\frac{\partial v}{\partial x} + \frac{\partial u}{\partial y}\right) & \frac{1}{2}\left(\frac{\partial w}{\partial x} + \frac{\partial u}{\partial z}\right) \\ \frac{1}{2}\left(\frac{\partial u}{\partial y} + \frac{\partial v}{\partial x}\right) & \frac{\partial v}{\partial y} & \frac{1}{2}\left(\frac{\partial w}{\partial y} + \frac{\partial v}{\partial z}\right) \\ \frac{1}{2}\left(\frac{\partial u}{\partial z} + \frac{\partial w}{\partial x}\right) & \frac{1}{2}\left(\frac{\partial v}{\partial z} + \frac{\partial w}{\partial y}\right) & \frac{\partial w}{\partial z} \end{bmatrix} \tag{3}$$

$$B = \frac{1}{2}(\nabla V - \nabla V^T) = \begin{bmatrix} 0 & \frac{1}{2}\left(\frac{\partial \mathrm{v}}{\partial \mathrm{x}} - \frac{\partial \mathrm{u}}{\partial \mathrm{y}}\right) & \frac{1}{2}\left(\frac{\partial \mathrm{w}}{\partial \mathrm{x}} - \frac{\partial \mathrm{u}}{\partial \mathrm{z}}\right) \\ \frac{1}{2}\left(\frac{\partial \mathrm{u}}{\partial \mathrm{y}} - \frac{\partial \mathrm{v}}{\partial \mathrm{x}}\right) & 0 & \frac{1}{2}\left(\frac{\partial \mathrm{w}}{\partial \mathrm{y}} - \frac{\partial \mathrm{v}}{\partial \mathrm{z}}\right) \\ \frac{1}{2}\left(\frac{\partial \mathrm{u}}{\partial \mathrm{z}} - \frac{\partial \mathrm{w}}{\partial \mathrm{x}}\right) & \frac{1}{2}\left(\frac{\partial \mathrm{v}}{\partial \mathrm{z}} - \frac{\partial \mathrm{w}}{\partial \mathrm{y}}\right) & 0 \end{bmatrix} \tag{4}$$

where $\| \|_F^2$ is the Frobenius norm; A is the symmetric part of the velocity gradient tensor and B is the anti-symmetric part, representing the deformation and rotation of a certain point in the flow field, respectively; ε is a small positive number to prevent division by zero and the value of ε is 0.001 in this paper. Extensive research has proven that the vortex structures can be effectively identified when $\Omega \geq 0.52$.

4. Result and discussion

4.1 Geometric Variation Induced by Transition Parameter T_r

The three-dimensional blade geometry is constructed from three defining streamwise layers (hub, center, shroud), with each layer's profile governed by the parametric equation (Eq. 1). In this parametric study, the turning parameter T_u was held constant at a value of 3 for all layers (T_{u1}, T_{u2}, T_{u3}) to isolate the effect of the transition parameter T_r. The initial baseline geometry was defined with all T_r values set to 2 (T_{r1}, T_{r2}, T_{r3}).

As illustrated in **Figure 4** for the hub layer, increasing T_{r1} transforms the transition segment from an inward-concave curvature ($T_{r1} = 0.5$) to a pronounced outward-convex shape. Higher values of T_{r1} (e.g., $T_{r1} = 1.5, 3,$ and 20) progressively sharpen this convex curvature, with extreme values ($T_{r1} = 20$) approaching a near-linear redirection. The optimization proceeded through layer-wise adjustment of these T_r values.

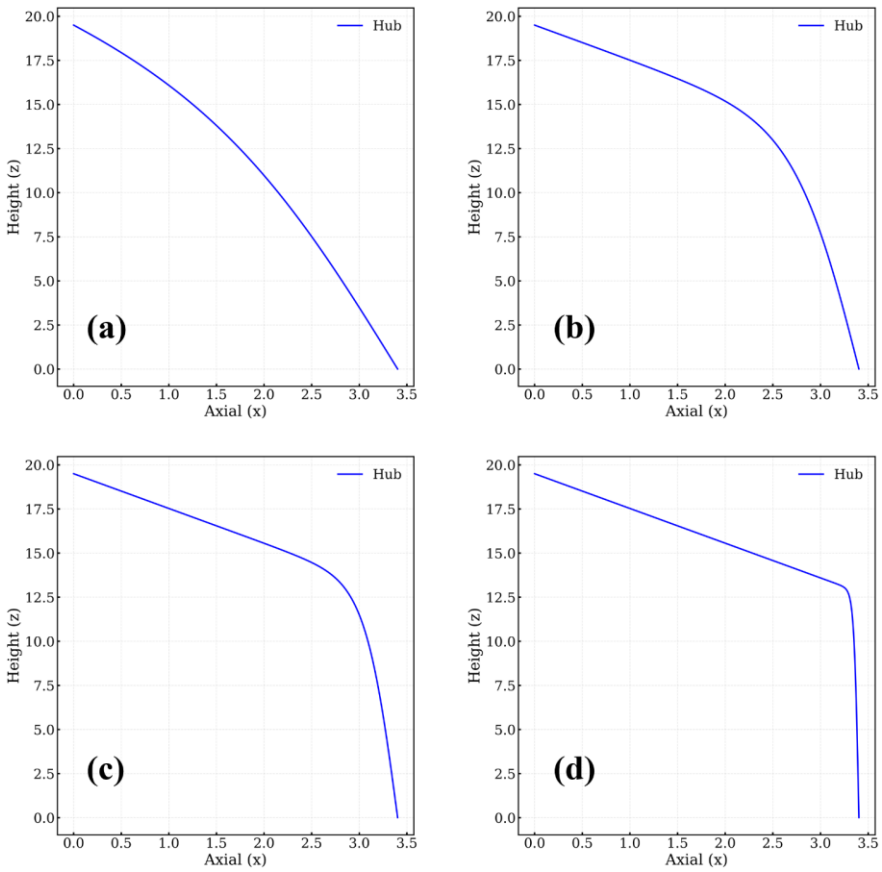

Figure 4. Effect of hub layer curvature parameter T_{r1} on blade profile geometry. (a) $T_{r1} = 0.5$ (inward-concave); (b) $T_{r1} = 1.5$; (c) $T_{r2} = 3$; (d) $T_{r3} = 20$ (outward-convex).

4.2 Sensitivity of Isentropic Efficiency to Layer-Specific T_r Values

A systematic parametric analysis was conducted to evaluate the sensitivity of isentropic efficiency (η_s) to variations in T_r at the hub (T_{r1}), center (T_{r2}), and shroud (T_{r3}) layers, starting from the initial uniform value of $T_r = 2$ for all layers. The results are summarized in **Figure 5**.

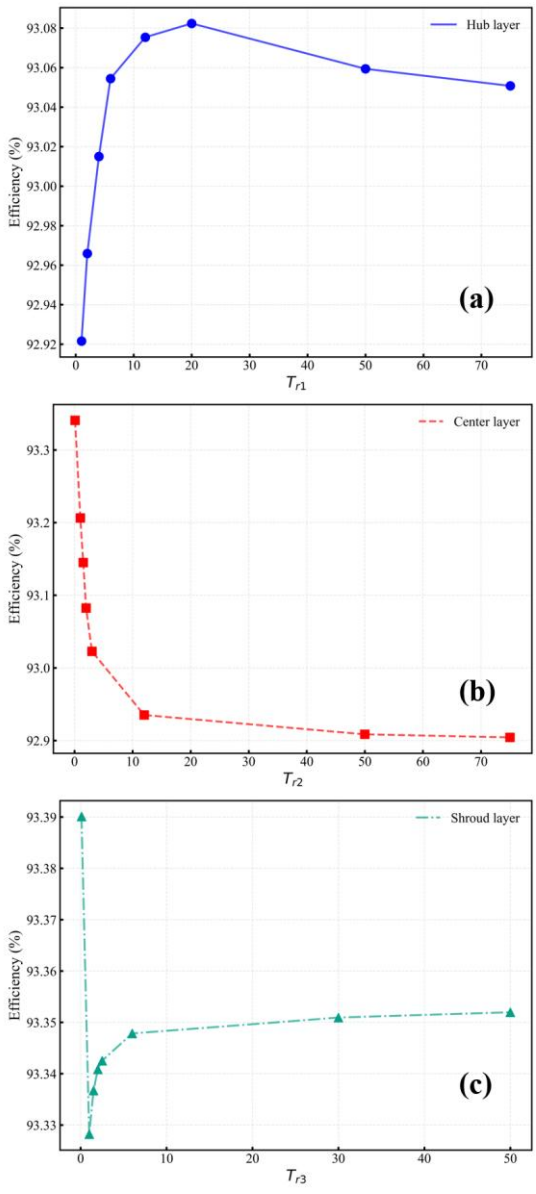

Figure 5. Isentropic efficiency sensitivity to T_r variations. (a) Hub (T_{r1}); (b) Center (T_{r2}); (c) Shroud (T_{r3}).

The optimization followed a sequential approach:

1. Hub layer optimization: With T_{r2} and T_{r3} fixed at 2, T_{r1} was varied. The analysis revealed a clear peak in efficiency at $T_{r1} = 20$.
2. Center layer optimization: With the optimized $T_{r1} = 20$ and $T_{r3} = 2$, T_{r2} was adjusted. The isentropic efficiency decreased monotonically with increasing T_{r2}, with the optimal performance achieved at a very low value of $T_{r2} = 0.1$. The variation range of efficiency

caused by adjusting T_{r2} was the largest among the three layers, underscoring its dominant influence.

3. Shroud layer optimization: Finally, with $T_{r1} = 20$ and $T_{r2} = 0.1$, T_{r3} was varied. The shroud layer exhibited minimal impact on overall efficiency ($\Delta\eta_s < 0.07\%$), and the optimal value was determined to be $T_{r3} = 0.1$.

This procedure yielded the final optimized parameter set: $T_{r1} = 20, T_{r2} = 0.1, T_{r3} = 0.1$.

As shown in **Figure 5(b)**, the isentropic efficiency decreases monotonically with increasing T_{r2}. The variation range of efficiency caused by adjusting T_{r2} is the largest among the three layers. This significant sensitivity underscores that the mid-span region, governed by the center layer profile, is critical for mainstream flow stability and loss generation. The optimal performance was achieved at a low T_{r2} value of 0.1, where the smooth curvature transition effectively suppresses secondary flows and vortex formation in this pivotal region.

In contrast, the shroud layer (T_{r3}) exhibited irregular efficiency fluctuations, potentially attributable to numerical convergence challenges during parameter adjustment. However, its absolute impact on efficiency remained negligible $\Delta\eta_s < 0.07\%$, confirming its marginal role in the core energy transfer process.

4.3 Performance Optimization and Flow Field Validation

Based on the parametric sensitivity analysis above, the optimal combination of transition parameters was determined as $T_{r1} = 20, T_{r2} = 0.1, T_{r3} = 0.1$. **Figure 6** presents the resulting three-dimensional impeller geometry generated by the CPPID method. The blade profile exhibits smooth curvature, particularly at the center region governed by the very low T_{r2} value, facilitating a gradual flow path transition from radial to axial orientation.

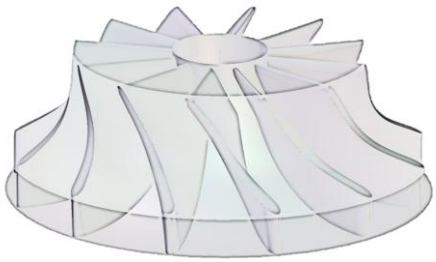

Figure 6. Cylindrical Projection-Based Parametric Impeller Design (CPPID)-optimized impeller.

The vortex structures within the flow passage were analyzed using the Ω method with a threshold of $\Omega = 0.8$ to highlight strong vortical regions. **Figure 7** compares the vortex distributions between the initial CPPID generated impeller, defined by the uniform parameters ($T_{r1} = 2, T_{r2} = 2, T_{r3} = 2$) which achieved an isentropic efficiency of 92.96%, and the final optimized CPPID impeller ($T_{r1} = 20, T_{r2} = 0.1, T_{r3} = 0.1$) with an efficiency of 93.39%. From the results, it can be observed that the middle layer of the optimized impeller blades exhibits an inward concave trend, which to a certain extent reduces the generation of intermediate eddies near the suction surface side.

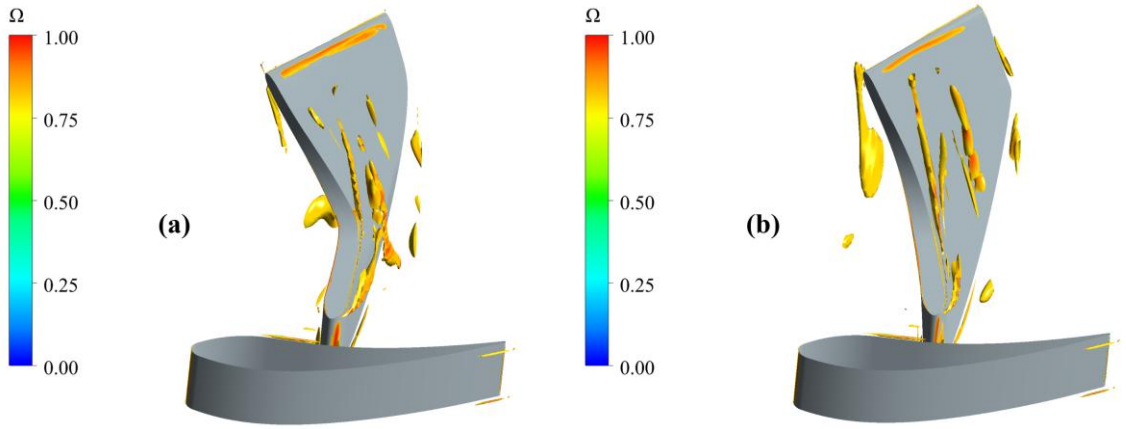

Figure 7. Comparison of vortex distributions ($\Omega = 0.8$) at 0.5 span (a) the initial CPPID impeller (b) the optimized CPPID impeller ($T_{r1} = 20, T_{r2} = 0.1, T_{r3} = 0.1$).

5. Conclusion

The CPPID framework enables a structured and layer-specific approach to impeller design. Through a sequential optimization of the transition parameters—from an initial uniform value($T_{r1} = 2, T_{r2} = 2, T_{r3} = 2, \eta_s = 92.96\%$) to an optimized set ($T_{r1} = 20, T_{r2} = 0.1, T_{r3} = 0.1, \eta_s = 93.39\%$). the method achieves a notable improvement in flow quality, as evidenced by the suppression of intermediate vortices near the suction surface side. This work establishes CPPID as a viable and systematic tool for designing high-efficiency impellers in cryogenic turbo-expanders, with potential applications in hydrogen liquefaction and other cryogenic systems.

Acknowledgments

This work is financially supported by the National Key Research and Development Program of China (No. 2021YFB4000700).

References

[1] Mayer T, Semmel M, Guerrero Morales MA, Schmidt KM, Bauer A, Wind J. Techno-economic evaluation of hydrogen refueling stations with liquid or gaseous stored hydrogen. International Journal of Hydrogen Energy. 2019;44(47):25809-33.

[2] Bauer A, Mayer T, Semmel M, Guerrero Morales MA, Wind J. Energetic evaluation of hydrogen refueling stations with liquid or gaseous stored hydrogen. International Journal of Hydrogen Energy. 2019;44(13):6795-812.

[3] Li X, Lv C, Yang S, Li J, Deng B, Li Q. Preliminary design and performance analysis of a radial inflow turbine for a large-scale helium cryogenic system. Energy. 2019;167:106-16.

[4] Zhu Z, Lou S, Zhang Y, An L, Liu Y, Li X. The design and research of two-stage series-connected helium turbine expanders for hydrogen liquefaction system. Applied Thermal Engineering. 2024;249.

[5] Liu H, Zuo J, Qiu S, Liang Y, Ke C, Liu L, et al. Simulative and experimental analysis of high-speed helium turbo-expanders in a 5t/day hydrogen liquefier. International Journal of Hydrogen Energy. 2025;133:152-64.

[6] Lu S, Wang Y, Jiang H, Li H, Ding L. Thermal concentration and cooling characteristics of a rotating turbine blade tip with different tip clearances. International Journal of Heat and Mass Transfer. 2026;254.

[7] Liu,Chaoqun,et al."Third generation of vortex identification methods: Omega and Liutex/Rortex based systems".Journal of Hydrodynamics,vol.31,2019,pp.205-223.